A neural network for identification and classification of systematic internal flaws in laser powder bed fusion

CIRP Journal of Manufacturing Science and Technology 37 (2022) 312–318

Contents lists available at ScienceDirect

CIRP Journal of Manufacturing Science and Technology

journal homepage: www.elsevier.com/locate/cirpj

A neural network for identification and classification of systematic internal flaws in laser powder bed fusion

Claudia Schwerz*, Lars Nyborg

Chalmers University of Technology, Department of Industrial and Materials Science, Sweden

ARTICLE INFO

Available online xxxx

Keywords:
In-situ monitoring
Powder bed fusion
Image analysis
Machine learning
Neural network classifier
Flaw detection
Defect detection
Lack of fusion
Porosity

ABSTRACT

Quality control of mechanical components is crucial to ensure their expected performance and prevent their failure. For components manufactured additively, quality control performed in-process is particularly interesting, as the sequential deposition and remelting of layers represent a possibility to mitigate existing flaws. The first step towards closed-loop control is to ensure that the monitoring setup and the data analytics approach can flag and discriminate flaws. This study aims to assess the potential of a layerwise monitoring system associated with a supervised machine learning approach to identify and classify internal flaws in laser powder bed fusion of Hastelloy X. For that, systematically generated internal flaws were mapped ex-situ in 72 distinct process conditions. The outputs of the near-infrared long-exposure acquisition system were labeled according to the ex-situ characterization and used to train a fully convolutional neural network. The network was then used to classify previously unseen monitoring images into three classes, according to the predominant flaw type expected, lack of fusion, keyhole porosity, or residual porosity. Accuracy, precision and recall over 96% are obtained, indicating that the monitoring system combined with this supervised machine learning approach successfully identifies and classifies internal flaws.

Introduction

The presence of flaws is inherent to any manufacturing process, including laser powder bed fusion (LPBF). While some flaws can be eliminated in post-processing, mechanical design often accounts for and admits flaws of restricted size and characteristics [1]. In order to identify whether a flaw is present in the material and assess its criticality, nondestructive inspection techniques, such as radiography and ultrasonic testing, are routinely employed industrially for flaw detection. However, these methods are typically performed ex-situ, post-manufacturing, and in these conditions cannot be used to identify or mitigate a flaw upon its formation. The advent of additive manufacturing introduces the possibility to mitigate flaws during the manufacturing process due to the layer-by-layer nature of the processes. This prospect, coupled with the need for identifying flaws and to the goal of implementing first-time-right manufacturing [2], gave rise to the enormous interest in in-situ monitoring and closed-loop control in the additive manufacturing community [3,4]. The capabilities of various sensors, monitoring setups and detection algorithms of detecting internal flaws, such as cracks, lack of fusion and pores, have been investigated in the literature.

Two of the most employed monitoring systems in LPBF are layerwise optical monitoring and real-time melt pool monitoring. The setup for optical monitoring of the powder bed typically consists of a camera that acquires signal in the visible spectrum across the entire build area in a layerwise fashion, after recoating or after laser exposure. In order to use this system for the detection of internal flaws, the in-situ detection is often validated by the ex-situ detection of flaws [5–7]. Process monitoring based on the acquisition of infrared emissions through photodiodes has been most widely used for thermal sensing but has also been applied to detect internal flaws in multilayer builds [8,9]. In this approach, as the monitoring is typically performed on the melt pool scale and with high acquisition rates, large amounts of data are generated. Similar to the approach employed in optical monitoring, process deviations are cross-checked ex-situ. Due to the reduced processing speed of this monitoring system, most of the research has been dedicated to identifying flaws in single tracks [10–12].

In LPBF process monitoring, there is a trade-off between processing time and resolution [13]. While layerwise signal acquisition,

* Correspondence to: Department of Industrial and Materials Science Chalmers University of Technology, Rännvägen 2, SE-412 96, Gothenburg, Sweden.
E-mail address: claudia.schwerz@chalmers.se (C. Schwerz).

https://doi.org/10.1016/j.cirpj.2022.02.010
1755-5817/

such as monitoring the powder bed through optical imaging, requires minimal computational efforts and data storage, it has limitations, especially on the scale of deviations that can be captured. On the other hand, real-time monitoring, such as thermal sensing with photodiodes, captures high-resolution data but demands great computational efforts and data storage. A promising alternative is a long-exposure thermal sensing system that acquires process signals during the entire process but yields a layerwise output covering the whole build area [14,15]. The resolution is sufficient to detect anomalies [16], while the layerwise output rate can be sufficient for mitigation to be performed in the subsequent layer. This setup has been employed to distinguish average pixel intensity values of images of specimens manufactured with standard process parameters and specimens with keyhole porosity and lack of fusion [17] and to monitor the process when an increasing number of layers are intentionally not exposed by the laser beam, resulting in insufficient binding [18]. Analysis of pixel intensity distribution was also used for determining which layers of prints with relatively complex geometries contain hotspots [19].

This study aims to assess the potential of using near-infrared long-exposure imaging with layerwise registration to discriminate regions of LPBF manufactured Hastelloy X that contain flaws from those virtually flaw-free and distinguish regions based on the predominant flaw type present. The assessment is based on images obtained from in-situ monitoring of the manufacturing process of specimens with varying flaw contents. As the flaws are generated systematically, their distribution is widespread throughout the material. Each monitored layer is used for training a neural network, which is then employed to classify images into containing a primary flaw type, lack of fusion, keyhole porosity or residual gas porosity only. This monitoring system has previously been demonstrated to detect flaws formed stochastically as a result of powder redeposition on the powder bed [16]. From an implementation perspective, using a single system capable of detecting multiple flaw types increases the control efficiency, hence the relevance of assessing the capabilities of this monitoring system to identify distinct flaw types.

Experimental setup and methods

Additive manufacturing and ex-situ classification per flaw type

In previous work by the authors [20], an EOS M290 (Electro Optical Systems GmbH, Germany) LPBF machine was employed to manufacture the material investigated in this study. The system is equipped with a Yb fiber laser with a maximum nominal power of 400 W and a focused beam diameter of 100 µm. The feedstock material utilized is gas atomized Hastelloy X (EOS NickelAlloy HX) powder with composition corresponding to UNS N06002 and particle size between 19 µm (d10) and 58 µm (d90).

The nominal laser power, scan speed and layer thickness were systematically varied to cover a comprehensive range of the process space, as shown in Table 1. Manufacturing was performed at a fixed hatch spacing, 100 µm. Each of the 72 sets of parameters was used to manufacture cylinder-shaped specimens of diameter 10 mm and height 20 mm, positioned on the build platform to avoid redeposition of process byproducts on the laser-exposed area, thereby avoiding the formation of spatter-driven stochastic flaws. Satisfactory recoating was ensured by monitoring the process with EOSTATE PowderBed monitoring, thereby avoiding the formation of stochastic flaws driven by powder bed inhomogeneities. All specimens were manufactured with a stripe exposure strategy, with a stripe width of 10 mm.

Table 1
Nominal process parameters employed in the manufacturing of Hastelloy X specimens.

Laser power (W)	100, 200, 300
Laser scan speed (mm/s)	200, 400, 600, 800, 1000, 1200, 1400, 1600
Layer thickness (µm)	20, 40, 80

In prior work [20], all specimens were characterized in terms of internal flaw content, flaw size distribution and predominant flaw type. The categorization per predominant flaw type is employed for labeling images in the present study.

In-situ monitoring and image acquisition

Monitoring of the manufacturing process was performed with the EOSTATE Exposure OT system, equipped with a 5-megapixel sCMOS (scientific complementary metal-oxide-semiconductor) camera positioned on top of the build chamber, covering the whole build platform area in its field of view. Multiple bandpass filters are employed to suppress the acquisition of signals extraneous to the built components, such as laser reflections and plasma emissions [14]. Hence the system only acquires signal from the process in a narrow range of the near-infrared spectrum, namely 887.5–912.5 nm. During the processing of each layer of the build, the system sequentially acquires images at 10 fps, pre-processes all the acquired images for noise reduction and geometric and intensity corrections, and outputs a single image. The intensity registered in each pixel corresponds to the maximum intensity registered in the 125 µm × 125 µm region of the build area corresponding to a pixel during the exposure of the layer. The acquisition is done in a layerwise fashion and, in the experiments performed in the present study, registers the signal obtained during the manufacture of multiple geometrically identical specimens of constant cross-section printed simultaneously. EOSTATE OT was employed for image acquisition only; all data processing and analysis was performed in a Matlab R2019b environment. After sectioning the acquired images into regions of constant size centered in the cross-section of each specimen, where only a single specimen can be observed, a database was constructed for training a neural network. The labeling is performed based on the ground-truth data obtained by ex-situ characterization.

Image analysis

To handle this classification problem, a supervised machine learning approach is taken. An annotated dataset is constructed and used to train, validate and test a fully convolutional neural network. Convolutional neural networks are powerful classifiers in which an input image undergoes sequential operations to finally be categorized into one of the pre-defined outputs [21]. On each convolutional layer, the data contained in the previous layer are linearly combined through convolution operations, then pass a batch normalization [22] step before introduction of non-linearity by the Rectified Linear Unit (ReLU) function:

$$f(x) = \max(x, 0) \tag{1}$$

In downsampling layers, max-pooling operations are performed with a stride length of two. In the penultimate layer of the network, class probabilities are estimated using the softmax function, which is a generalization of the logistic sigmoid function for a multiclass problem:

$$f_i(x) = \frac{\exp(x_i)}{\sum_j \exp(x_j)} \tag{2}$$

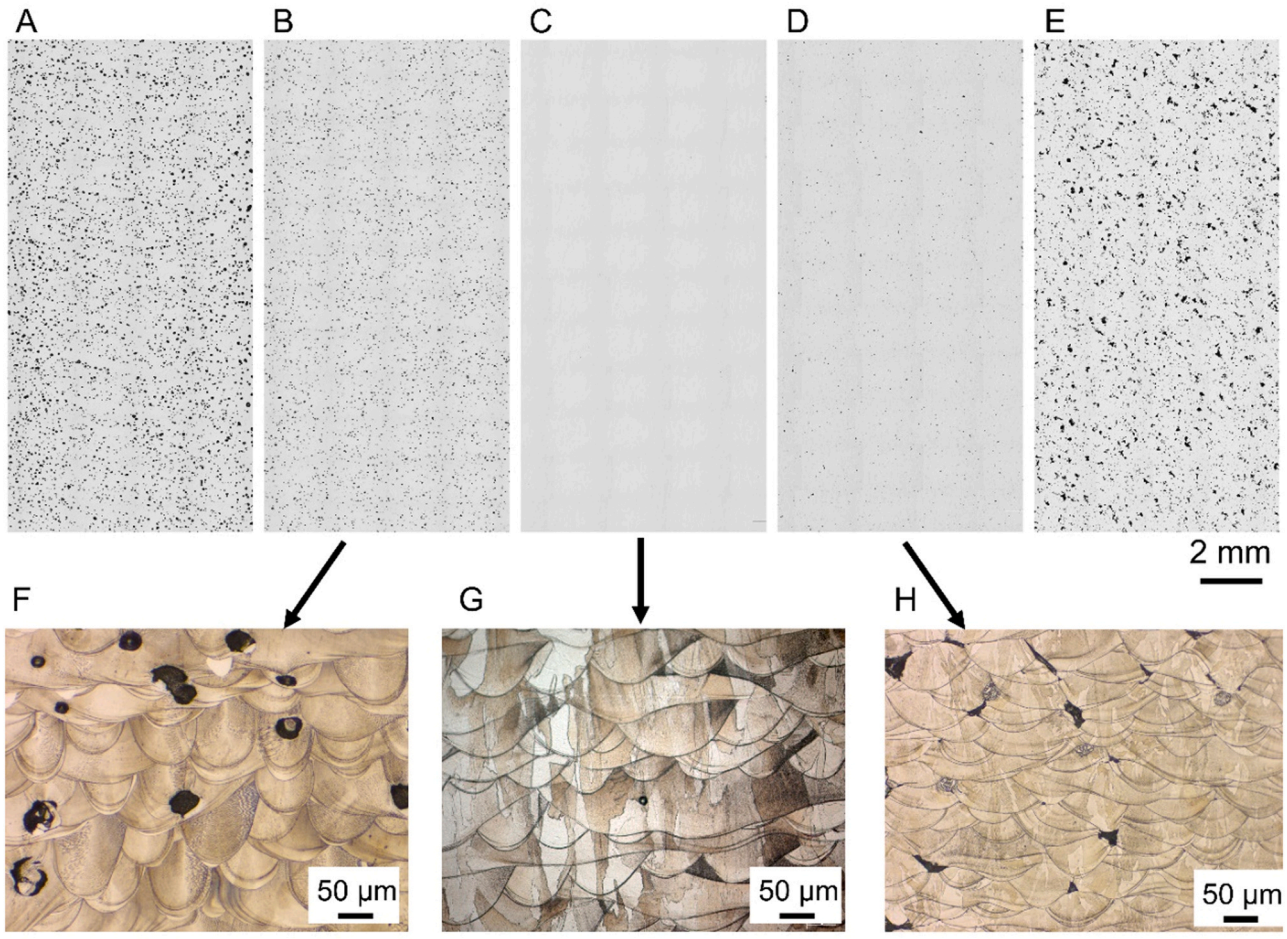

Fig. 1. Overview of the deliberately generated systematic flaws. (A) and (B) show cross-sections with different volume fractions of systematic keyhole porosity. A detailed sample of keyhole porosity is observed in (F). (C) represents a sample virtually free from flaws, in which only gas porosity has been identified. A sample of gas porosity is seen in (G). (D) and (E) show cross-sections with distinct volume fractions of systematic lack of fusion. A detailed sample of lack of fusion is observed in (H).

Results

Ex-situ characterization

As the flaws observed in this study are generated as a result of the selection of process parameters, their occurrence is systemic, and their distribution is homogeneous, as observed in the cross-sections in Fig. 1. The figure illustrates the variability of the internal flaw populations generated through the experimental design. Fig. 1 A-B represent different levels of systematic keyhole porosity, a flaw type obtained when excessive energy is input to the material. The material illustrated in A has received a higher energy input in its manufacturing than B and presents larger size and volume fraction flaws. Fig. 1 C represents a specimen where only residual gas porosity was identified, which corresponds to the case in which the material is virtually flaw-free as a result of adequate energy input in the manufacturing process. Fig. 1 D-E illustrate systematic lack of fusion with varying degrees of severity as a result of progressively lower energy input.

Small, spherical and sparse pores are always present in as-printed LPBF material due to the gas entrapped in the feedstock powder [23] and solubility drop of gas-forming elements present in the feedstock powder upon solidification [24,25]. Hence, “residual porosity” corresponds to desirable processing conditions and will only be considered the predominant flaw type if no other flaws are present. The predominant flaw types identified in each of the 72 specimens in [20] are shown in Fig. 2.

Flaw types and construction of the dataset

The dataset used to train, validate, and test the network was constructed with near-infrared long-exposure images obtained layerwise from the cylindrical specimens built employing the parameters in Table 1. Patches of dimensions 81 × 81 pixels centered in the specimen layerwise cross-sections were obtained from each image and labeled according to the predominant flaw type previously determined through metallographic analysis. As the flaws are generated systematically due to the selection of process parameters and occur systemically in the microstructure, each layer is assumed to be representative of the resulting flaw distribution. A total of 38,097 labeled images were obtained, out of which 8709 were assigned the label “keyhole porosity”; 21,909, “lack of fusion”; 7479, “residual porosity”. Sample images obtained from three specimens belonging to the distinct categories are visualized in Fig. 3, in which four distinct layers are depicted. The striped artifacts present in the sample images result from the laser scanning pattern and data collection gap of the system, and vary layer by layer in a single specimen due to the rotation of the stripe pattern and the varying stripe layout on the laser exposure. The disruptions in the striped pattern mark the locations of stripe overlaps.

To ensure a balanced and varied dataset, the 7479 images labeled “residual porosity” were included in the dataset, and, for the remaining categories, the same number of labeled images were randomly selected to compose the dataset. Hence, the effectively

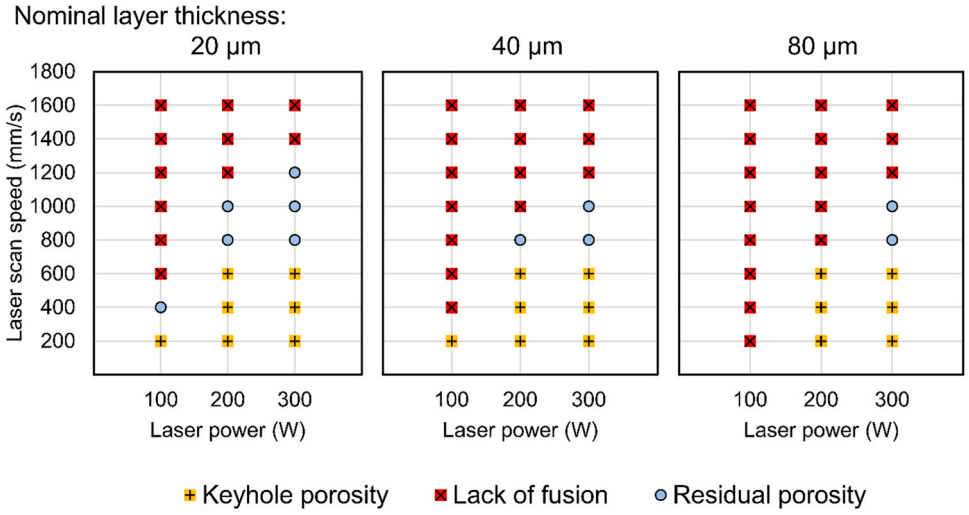

Fig. 2. Predominant flaw type in Hastelloy X across the process space, based on ex-situ characterization. Based on data collected in [20].

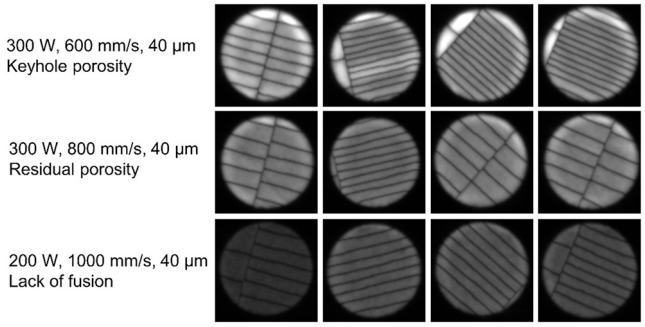

Fig. 3. Image patches obtained from three specimens containing distinct predominant flaw types. The process parameters employed in manufacturing are indicated. Four distinct layers are represented.

utilized dataset contains 22,437 labeled images equally divided into three categories.

Network architecture

A fully convolutional neural network was designed to classify images per primary flaw type identified through metallographic analysis. This choice was made as a fully convolutional neural network can process inputs of any dimensions, despite the training being performed on images of fixed size, and is the architecture suitable for semantic segmentation, which enables the application of the trained network to any part geometry. Training and validation were performed in the dataset built as per the previous section. The network layers were designed to handle the 81×81 inputs and reduce their dimensions gradually through convolution and max-pooling operations, followed by a final convolutional layer that results in an output of dimensions $1 \times 1 \times 3$. This way, the fully connected layer typically present in the last steps of a neural network is replaced by a convolutional layer that produces an output of the same dimension, which is dependent on the number of classes, in this case, three. This layer is then used as an input to the Softmax layer. Finally, a classification layer is used to output a predicted class, "keyhole porosity", "lack of fusion" or "residual porosity".

The network was designed to contain adequate complexity to avoid overfitting while being relatively simple. For that, a limited number of parameters were used, still ensuring satisfactory validation accuracy. Moreover, three max-pooling layers were used to decrease spatial resolution, thereby decreasing computational time. In order to improve training, batch normalization layers were added. The network can be schematically visualized in Fig. 4.

Experimental evaluation of the network

The dataset was split into training, validation, and test data at ratios 75%, 20% and 5%, respectively. The training was performed with stochastic gradient descent with momentum, at a fixed

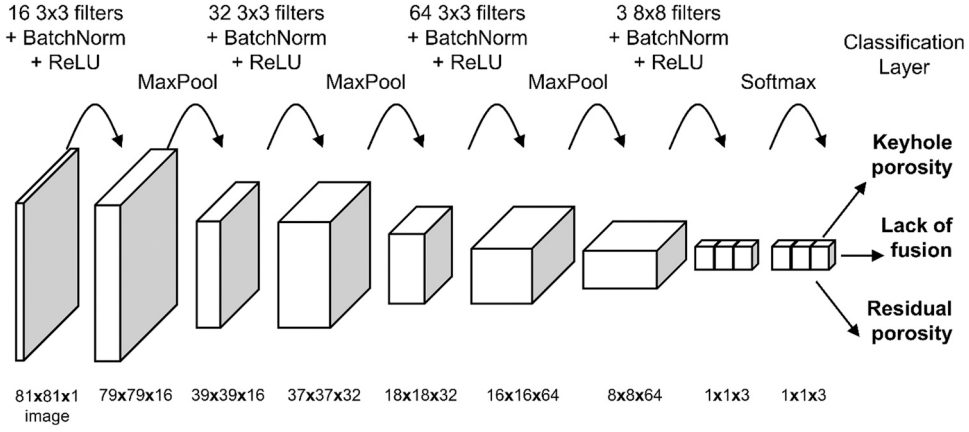

Fig. 4. Schematic of the network architecture. The layers in the network are represented together with their inputs and outputs.

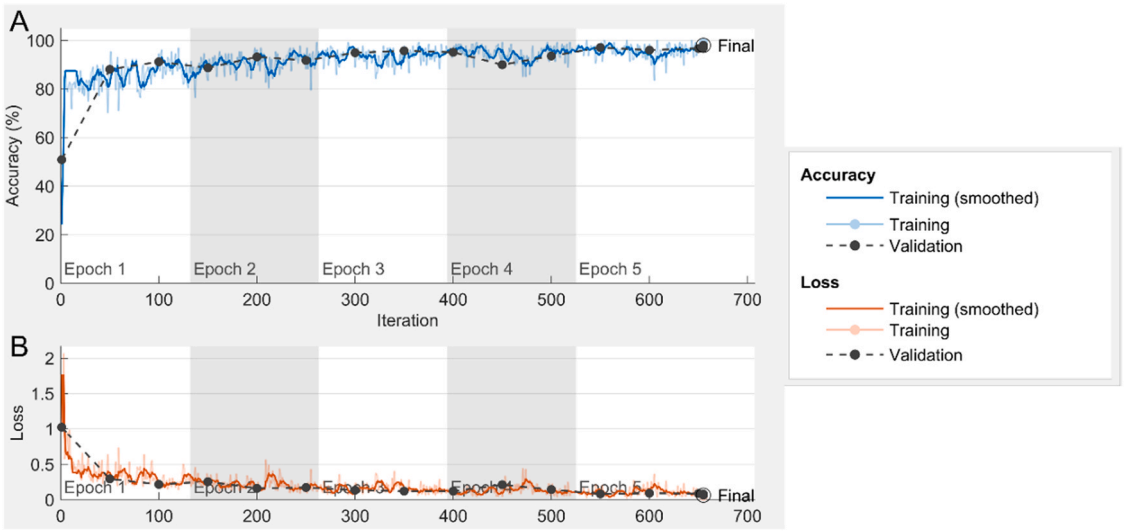

Fig. 5. Training progress plots. (A) shows increasing prediction accuracy in the training and validation sets. (B) shows decreasing loss function in the training and validation sets.

learning rate of 0.01, and L2 regularization factor of 1.0e-4. The training was stopped after five epochs since the accuracy of the network had already reached a plateau at that point, as well as the loss function for the validation dataset, indicating no overfitting. The training and validation losses, as well as the accuracies, are shown in Fig. 5. The resulting validation accuracy is 97.99%.

The network was employed to classify the 1122 images previously set apart in a test set. These images are previously unseen by the network, and can therefore be used to estimate its performance in practice. The performance of the model is described in the confusion matrix in Fig. 6, in which the rows represent the class predicted by the network, and the columns represent the true class, which corresponds to the label assigned during the construction of the dataset. The diagonal cells, in green, present the total number and percentage of the total number of observations classified correctly for each class, while the remaining cells, in red, correspond to incorrect classifications. Precision and false discovery rates correspond to the percentages of images predicted to belong to each class that are correctly and incorrectly classified, respectively, and are shown in the column on the far right. Recall and false-negative rates correspond to the percentages of images belonging to each class that are correctly and incorrectly classified, respectively, and are shown in the bottom row.

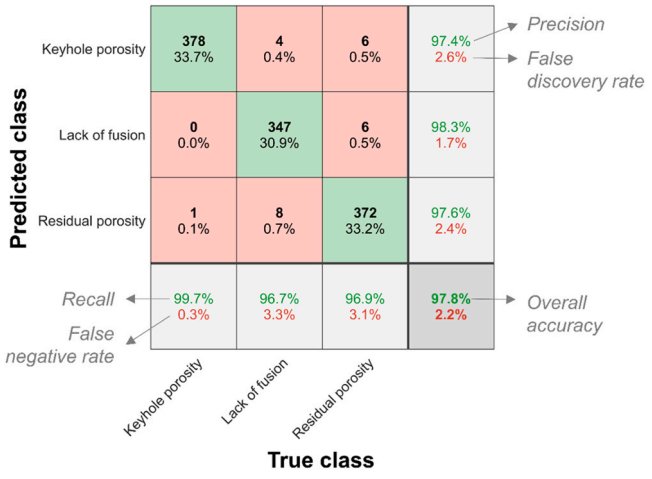

Fig. 6. Confusion matrix showing the performance of the network in classifying the 1122 images in the test set.

Discussion

In this study, an sCMOS camera integrated with a bandpass filter was employed to acquire long-exposure images of the entire LPBF build area when manufacturing specimens through 72 distinct process conditions. The specimens either contain systematic lack of fusion and keyhole porosity of varying degrees of severity, or are virtually free from flaws, in which case only residual gas porosity is present. The acquired images were utilized for training, validating and testing a convolutional neural network that predicts the predominant flaw type, given an image obtained in-situ.

A 5 Megapixel sCMOS camera with a field of view comprising the entire build area was used for signal acquisition. The narrow spectral range allowed by the filter integrated into the camera ensures that most noise characteristic to the LPBF process is eliminated, which is a major concern for the robustness of the monitoring system. The increased shutter time boosts the pixel intensities, counteracting the large field of view and the narrow bandwidth, and highlights heat sink regions, where flaws are prone to be formed [16]. Even though the acquisition is performed at 10 fps, the system combines the images acquired in a layer into a single output image [15]. On the one hand, the reduced output of the system makes it suitable as a quality control tool due to the increased data processing speed and the reduced storage needs, which facilitates traceability in an industrial environment, for example. On the other hand, layerwise monitoring implies that corrective actions cannot be taken immediately, as would be feasible in real-time monitoring, but only upon completion of the exposure of the layer. Considering the additive nature of the process, i.e., sequential deposition of layers, several layers are remelted in each pass, thus enabling the healing of flaws. In this perspective, layerwise monitoring might suffice for detection and mitigation of internal flaws, and consititutes a feasible alternative to real-time monitoring, which requires processing of large volume of data.

Before a monitoring system can be used as a quality assurance tool, it must be calibrated to ensure a fair correspondence between detections and flaws of interest. An approach taken in more mature inspection systems is to generate flaws of controlled dimensions at pre-defined locations, for example, by drilling holes in the material and calibrating the detection system to generate a distinct signal on those locations [26]. In AM, the goal is in-situ detection of flaws; therefore, the flaws created deliberately to test the monitoring system must be created in-situ, and the method for the deliberate generation of flaws becomes an issue to be considered. Some flaws

arise in laser powder bed fusion (LPBF) stochastically, for example, due to spatter redeposition on the powder bed. Flaws formed through this mechanism were successfully detected through the same monitoring system employed in the present study [16] but consisted of lack of fusion flaws driven by spatter redeposition only. Thus, the monitoring system had not yet been proven to detect other flaw types, such as keyhole pores. This flaw type, as well as lack of fusion, was intentionally generated in this study from improper selection of process parameters. Other flaw types can occur in materials manufactured via LPBF, as a result of improper design [27]. Detection of these flaws is not in the scope of this work.

In practice, sub-optimal parameters are likely not employed in manufacturing, as the manufacturing process is preceded by extensive research and development. However, regions of heat accumulation and internal flaws can occur depending on part geometry and scan strategy [28], particularly in regions where short hatch vectors are present [29]. In this sense, the strategy for deliberate flaw generation implemented in this study mimics a pore formation process that occurs in practice. For the case of systematic lack of fusion, the extensive process mapping and metallography work has identified systematic lack of fusion in varied conditions, including those where high relative density is obtained, which tend to be overlooked in the optimization process due to the use of relative density as processability metric. The model correctly predicted these conditions. The trained model can be used to detect regions of lack of fusion due to fluctuations in the laser intensity, particularly in manufacturing conditions that produce melt pools with low marginals in relation to geometrical parameters (width and depth with dimensions close to hatch spacing and layer thickness, respectively).

Conclusions

In this study, a sizeable dataset (38,097 labeled images) was created from images obtained through in-situ monitoring of the LPBF process during the manufacture of Hastelloy X specimens. The manufacturing process was designed to comprise ample process conditions and varied flaw contents. A fully convolutional neural network was trained and was deemed capable of determining the predominant flaw type based an image obtained through in-situ monitoring. Best machine learning practices were employed to assure the robustness of the model.

It is demonstrated that the fully convolutional neural network trained on near-infrared long-exposure images is capable of classifying individual layers of specimens per predominant flaw type in the categories *keyhole porosity*, *lack of fusion*, and *residual porosity* with high accuracy (97.8% in the test set), precision and recall (above 96% for all classes), when considering systematic process parameter-induced flaws.

Declaration of Competing Interest

The authors declare that they have no known competing financial interests or personal relationships that could have appeared to influence the work reported in this paper.

Acknowledgments

This work was conducted within the framework of the project MANUELA - Additive Manufacturing using Metal Pilot Line, funded by European Union's Horizon 2020 research and innovation programme under grant agreement no. 820774. The authors would also like to acknowledge the Centre for Additive Manufacturing – Metal (CAM2), supported by the Swedish Governmental Agency of Innovation Systems (Vinnova). The authors would like to thank Electro Optical Systems Finland Oy for providing the feedstock powder utilized in this research and the Production Area of Advance, Chalmers University of Technology.

References

[1] Beretta, S., Romano, S., 2017, A Comparison of Fatigue Strength Sensitivity to Defects for Materials Manufactured by AM or Traditional Processes. International Journal of Fatigue, 94:178–191. https://doi.org/10.1016/j.ijfatigue.2016.06.020.
[2] Colosimo, B.M., Grasso, M., 2020, In-situ Monitoring in L-PBF: Opportunities and Challenges. Procedia CIRP, 94:388–391. https://doi.org/10.1016/J.PROCIR.2020.09.151.
[3] Renken, V., Albinger, S., Goch, G., Neef, A., Emmelmann, C., 2017, Development of an Adaptive, Self-learning Control Concept for an Additive Manufacturing Process. CIRP Journal of Manufacturing Science and Technology, 19:57–61. https://doi.org/10.1016/J.CIRPJ.2017.05.002.
[4] Mazumder, J., 2015, Design for Metallic Additive Manufacturing Machine with Capability for "Certify as You Build. Procedia CIRP, 36:187–192. https://doi.org/10.1016/J.PROCIR.2015.01.009.
[5] Lu, Q.Y., Nguyen, N.V., Hum, A.J.W., Tran, T., Wong, C.H., 2020, Identification and Evaluation Defects in Selective Laser Melted 316 L Stainless Steel Parts Via In-situ Monitoring and Micro Computed Tomography. Additive Manufacturing, 35:101287https://doi.org/10.1016/j.addma.2020.101287.
[6] Gobert, C., Reutzel, E.W., Petrich, J., Nassar, A.R., Phoha, S., 2018, Application of Supervised Machine Learning for Defect Detection during Metallic Powder Bed Fusion Additive Manufacturing using High Resolution Imaging. Additive Manufacturing, 21:517–528. https://doi.org/10.1016/j.addma.2018.04.005.
[7] Imani, F., Gaikwad, A., Montazeri, M., Rao, P., Yang, H., Reutzel, E., 2018, Process Mapping and In-process Monitoring of Porosity in Laser Powder Bed Fusion using Layerwise Optical Imaging. Journal of Manufacturing Science and Engineering, Transactions of the ASME, 140. https://doi.org/10.1115/1.4040615.
[8] Bisht, M., Ray, N., Verbist, F., Coeck, S., 2018, Correlation of Selective Laser Melting-melt Pool Events with the tensile properties of Ti-6Al-4V ELI processed by laser powder bed fusion. Additive Manufacturing, 22:302–306. https://doi.org/10.1016/j.addma.2018.05.004.
[9] Coeck, S., Bisht, M., Plas, J., Verbist, F., 2019, Prediction of Lack of Fusion Porosity in Selective Laser Melting based on Melt Pool Monitoring Data. Additive Manufacturing, 25:347–356. https://doi.org/10.1016/j.addma.2018.11.015.
[10] Forien, J.B., Calta, N.P., DePond, P.J., Guss, G.M., Roehling, T.T., Matthews, M.J., 2020, Detecting Keyhole Pore Defects and Monitoring Process Signatures during Laser Powder Bed Fusion: A Correlation between In Situ Pyrometry and Ex Situ X-ray Radiography. Additive Manufacturing, 35. https://doi.org/10.1016/j.addma.2020.101336.
[11] Scime, L., Beuth, J., 2019, Using Machine Learning to Identify In-situ Melt Pool Signatures Indicative of Flaw Formation in a Laser Powder Bed Fusion Additive Manufacturing Process. Additive Manufacturing, 25:151–165. https://doi.org/10.1016/j.addma.2018.11.010.
[12] Zhang, Y., Hong, G.S., Ye, D., Zhu, K., Fuh, J.Y.H., 2018, Extraction and Evaluation of Melt Pool, Plume and Spatter Information for Powder-bed Fusion AM Process Monitoring. Materials & Design, 156:458–469. https://doi.org/10.1016/j.matdes.2018.07.002.
[13] Chua, C.K., Wong, C.H., Yeong, W.Y., 2017, Process Control and Modeling. Stand. Qual. Control. Meas. Sci. 3D Print. Addit. Manuf.. Elsevier: 159–179. https://doi.org/10.1016/b978-0-12-813489-4.00007-6.
[14] J. Bamberg, G. Zenzinger, A. Ladewig, In-Process Control of Selective Laser Melting by Quantitative Optical Tomography, in: 19th World Conf. Non-Destructive Test., 2016: pp. 1–8. https://doi.org/10.2110/palo.2006.p06–040r.
[15] G. Zenzinger, J. Bamberg, A. Ladewig, T. Hess, B. Henkel, W. Satzger, Process Monitoring of Additive Manufacturing by using Optical Tomography, in: AIP Conf. Proc., 2015: pp. 164–170. https://doi.org/10.1063/1.4914606.
[16] Schwerz, C., Raza, A., Lei, X., Nyborg, L., Hryha, E., Wirdelius, H., 2021, In-situ Detection of Redeposited Spatter and its Influence on the Formation of Internal Flaws in Laser Powder Bed Fusion. Additive Manufacturing:102370https://doi.org/10.1016/J.ADDMA.2021.102370.
[17] Mohr, G., Altenburg, S.J., Ulbricht, A., Heinrich, P., Baum, D., Maierhofer, C., Hilgenberg, K., 2020, In-situ defect detection in laser powder bed fusion by using thermography and optical tomography—comparison to computed tomography. Metals, 10:103. https://doi.org/10.3390/met10010103.
[18] Ulbricht, A., Mohr, G., Altenburg, S.J., Oster, S., Maierhofer, C., Bruno, G., 2021, Can Potential Defects in LPBF Be Healed from the Laser Exposure of Subsequent Layers? A Quantitative Study. Metals, 11:1012. https://doi.org/10.3390/met11071012.
[19] Yadav, P., Singh, V.K., Joffre, T., Rigo, O., Arvieu, C., Le Guen, E., Lacoste, E., 2020, Inline Drift Detection Using Monitoring Systems and Machine Learning in Selective Laser Melting. Advanced Engineering Materials, 22:2000660https://doi.org/10.1002/adem.202000660.
[20] Schwerz, C., Nyborg, L., 2021, Linking In Situ Melt Pool Monitoring to Melt Pool Size Distributions and Internal Flaws in Laser Powder Bed Fusion. Metals, 11:1856. https://doi.org/10.3390/MET11111856.
[21] LeCun, Y., Bottou, L., Bengio, Y., Haffner, P., 1998, Gradient-based Learning Applied to Document Recognition. in: Proceedings of the IEEE, 86:2278–2323. https://doi.org/10.1109/5.726791.
[22] S. Ioffe, C. Szegedy, Batch Normalization: Accelerating Deep Network Training by Reducing Internal Covariate Shift, 32nd Int. Conf. Mach. Learn. ICML 2015. 1 (2015) 448–456. ⟨https://arxiv.org/abs/1502.03167v3⟩ (Accessed August 2, 2021).

[23] Aboulkhair, N.T., Everitt, N.M., Ashcroft, I., Tuck, C., 2014, Reducing Porosity in AlSi10Mg Parts Processed by Selective Laser Melting. Additive Manufacturing, 1:77–86. https://doi.org/10.1016/j.addma.2014.08.001.
[24] Snow, Z., Nassar, A.R., Reutzel, E.W., 2020, Invited Review Article: Review of the Formation and Impact of Flaws in Powder Bed Fusion Additive Manufacturing. Additive Manufacturing, 36. https://doi.org/10.1016/j.addma.2020.101457.
[25] Kou, S., 2003, Welding Metallurgy. 2nd ed. John Wiley & Sons, Inc.. https://doi.org/10.1002/0471434027.
[26] Shull, P.J., 2001, Nondestructive Evaluation - Theory, Techniques, and Applications. CRC Press. https://doi.org/10.1201/9780203911068.
[27] Grasso, M., Colosimo, B.M., 2017, Process Defects and in Situ Monitoring Methods in Metal Powder Bed Fusion: A Review. Measurement Science and Technology, 28:aa5c4fhttps://doi.org/10.1088/1361-6501/aa5c4f.
[28] Zhang, B., Li, Y., Bai, Q., 2017, Defect Formation Mechanisms in Selective Laser Melting: A Review. Chinese Journal of Mechanical Engineering (English Edition), 30:515–527. https://doi.org/10.1007/s10033-017-0121-5.
[29] Diehl, B., Nassar, A., 2020, Reducing Near-surface Voids in Metal (Ti-6Al-4V) Powder Bed Fusion Additive Manufacturing: The Effect of Inter-hatch Travel Time. Additive Manufacturing, 36. https://doi.org/10.1016/j.addma.2020.101592.